



Research Article

Numerical investigation to augmentation of heat transfer in solar air heater with arc shape ribs on absorber plate

Ghaith Monem FADALA^{1,*}, Ahmed Hashem YOUSEF², Karrar S. HASAN¹

¹Engineering Technical College, Al-Furat Al-Awsat Technical University, Al-Najaf, 31001, Iraq

²Al-Diwaniyah Technical Institute, Al-Furat Al-Awsat Technical University, Al Diwaniyah, 31001, Iraq

ARTICLE INFO

Article history

Received: 25 May 2023

Revised: 17 October 2024

Accepted: 18 October 2023

Keywords:

Artificial Roughness; CFD, Fluid Flow; Heat Transfer; Solar Air Heater; Solar Energy

ABSTRACT

Using numerical methods, this paper investigates the heat transmission and friction factor of a SAH duct that has been intentionally roughened. The absorber plate of the duct is equipped with an arc-shaped structure that has three distinct angles of attack. This structure is installed on the peak walls from the tray. The roughness parameters of this structure include a respective roughness factor (p/H) beginning from 1.667 to 6.667, a respective rough height (e/H) of 0.271, an arc angle (α) beginning from 30° to 60°, and a Re beginning from 3000 to 15000. It has been determined that the efficiency of roughened SAH ducts surpasses that of smooth ducts within the range of roughness values examined. The numerical analysis indicates that the highest increase in Nu and f occurred at specific values: a respective roughness factor (p/H) of 3.33, a respective roughness height (e/H) of 0.271, an arc angle (α) of 60°, and a Reynolds number of 15000. The test runs for the roughened duct involved collecting data on various combinations of roughness parameters. The highest values observed were $Nu = 215$ and Nu ratio = 7.21. When compared to the conduit that is smooth had most possible value of $f = 2.5$ and $f/f_s = 3.39$. The thermal performance factor is 3.88.

Cite this article as: Fadala GM, Yousef AH, Hasan KS. Numerical investigation to augmentation of heat transfer in solar air heater with arc shape ribs on absorber plate. J Ther Eng 2025;11(1):25–39.

INTRODUCTION

Due to its abundance and excellent quality, solar power has the ability to fulfill the modern world's energy demands with little negative impacts on the environment. Optimal performance of technologically advanced usage of solar energy certain pieces of machinery demand high-quality energy; the sun supplies more power to earth in more energy is consumed by the human population in a single

hour than the entire population consumes in a single year. In comparison to other sources of power, solar power has the distinct advantage of not adding to environmental pollution [1-2]. It was necessary to go to an alternative solution, which is renewable energy [3-6], which is considered one of the most important resources in the future if it is used, exploited, and worked on properly. Research is being conducted on solar energy and its applications to benefit from

*Corresponding author.

*E-mail address: gaith7751@gmail.com, gaith.tw1997@gmail.com

This paper was recommended for publication in revised form by Editor-in-Chief Ahmet Selim Dalkılıç



it in various aspects of life, so solar air heaters are among the available applications that are easy to use, clean, and environmentally friendly, and last for a period because they are cheap and non-polluting. It is one of the uses of drying crops, heating homes and reheating production lines, and therefore it is fruitful [7, 8]. One drawback that accompanies these applications is the low heat transfer efficiency. Therefore, Utilization of synthetic It is rough. to Increment its efficiency is one of the applications that increment the heat transfer rate of the SAH themselves. The researchers directed the use of these applications to improve SAH. In order to enhance the functionality of SAH, there are a number of novel approaches. One of these methods is through the fins extended on the surface in a wavy shape, the second is through artificial roughness placed on the absorbent surface, and this technique is considered the most acceptable by many researchers. Garg [9] introduced the traditional SAH as a rough rectangular duct with three parts: an inlet, a test section, and an exit point. Jovini et al. [10] presented a test of hypotheses on the improvement of the Nusselt number of SP- solar air heaters, using different spring parameters coil diameter (2.5,5,7.5) mm, wire diameter (0.5,1,1.5) mm and step (2.5, 5,7.5) mm, where the researchers explained that the use of such roughness causes heat transmission to be more valuable, Compared to axial flow, the cross-flow pattern that is achieved is higher. Where the Nu increases by (4.67-3.11) and (18.81-5.01) for cross-flow areas, but for axial flow, the value of the Nusselt number is (3.12-5.59) and (7.51-28.39). One of the new methods mentioned is the manufacture of protrusions on the absorbent plate to improve heat transfer [11, 12]. Subsequently, SAH was developed and improved using the technique for surface roughness on absorbent materials by a number of researchers to gain access to a set of special information about artificial roughness. Review the references reached by the researchers [13, 15]. Chand et al. [16] a numerical study was presented using 2D CFD of a rectangular channel SAH with artificial roughness in the presence of vortex generators on three types: rectangular, triangle, and circular, with artificial roughness parameters of Re 3800–18000 and heat flow of 1100 W/m². ANSYS 16 software was used to examine the variance in the Nusselt mean with the change of Re. It was found that the Nusselt rate increased with the presence of triangular vortices with little pressure loss. At Re = 3800, triangular vortices had the best thermal coefficient performance. Yadav and Sharma [17] experiment was carried out with the addition of a mixture of triangular ribs on an absorbent plate to a SAH with parameters Re = 3000-18000, e/D =0.045, and P/e =5-12.5. The study seeks in order to discover the influence of the step on both heat transmission and friction. Compared to the smooth layer, the most advanced level of thermal efficiency was attained at P/e = 10 by 2.02, the Nu was 3.05 and the coefficient of friction was 4.14. Jin et al. [18] a numerical analysis was conducted in order to investigate the properties of heat transmission and flux using various V-shaped roughness

parameters. The study determined that at the temperature, the thermal performance coefficient was found to be excellent. a P/e ratio of 10, with a value of 2.35. Luo et al. [19] a study on solar air heaters using dimple and delta winglet VGs showed a 36.23% improvement in heat transfer and a 36.29% friction factor. Tamna et al. [20] the thermal properties of a staggered V baffled absorbent plate (SAH) with artificial roughness were investigated in the study, where the lowest step, $P_R = 0.5$, achieves optimal thermal efficiency. Fadala et al. [21] a review study showing ways to improve heat transfer using synthetic fillers for a solar air heater. Where the research dealt with aspects, including the use of artificial roughness technique after its types, as well as impact of bilateral and unilateral efficiency of the process of SAH. The inclusion of RWVG led to a thermal enhancement (TEF) in their research. Zhang et al. [22] researchers found that a new VG, placed inside a helical channel, enhances heat transmission with minimal pressure loss, highlighting the importance of VG installation in enhancing heat transfer. Gupta et al. [23] according to the research, punched RWVG greatly enhanced heat transfer in fin-and-tube heat exchangers, which frequently led to a reduction in pressure. Li et al. [24] the study investigated the effects of increasing pressure drop on the pumping power and heat transfer in a fin-and-tube heat exchanger, hence improving its thermal-hydraulic efficiency. Promvong et al. [25] researchers looked at the thermo-hydraulic efficiency of two different configurations of vortex generators—one with rectangular blades and one with delta winglets—and found that the V-shaped delta winglet VG was marginally more effective.

According to studies, solar air heating (SAH) can have better thermal performance if its surface is artificially roughened with ribs. A number of earlier investigations investigated the impact of height in relation to the roughness by altering the side form to a circle, rectangle, triangle, semicircle, or NACA shape. But this research intends to close that knowledge gap by looking at how these variables affect the flow and heat transfer properties of the collector. The study explores the possibility of using arc-shaped ribs that can reach a height of 1.2 cm to improve the heat efficiency of a SAH, even when the coefficient of friction increases, resulting in more pumping power.

NUMERICAL MODELING

Geometrical Modeling and Mesh

A SP-SAH with artificial roughness was modeled in three dimensions using SolidWorks 2021 software. The resulting data was converted to ANSYS DESIGN MODELER 17 for investigation of the heat transfer rate. Figure 1 shows a demonstration of the SAH duct. The channel is separated into three portions based on its length. L1=600 mm entry, L2=1200 mm test, L3=300 mm exit, W=300mm, and H=30mm high. Step p = 5–20 cm has four

values, and the angles of attack are 30°, 45°, and 60°. In addition, $Re=3000-15000$ with 4 values. The aluminum absorber plate featured in Table 1 has a thickness of 0.5 mm, an arc of artificial roughness, and a heat flux of 1000 W/m^2 .

Test Independent of Infrastructure

During a quantitative investigation, obtaining an accurate the outcome of Nu and for the proposed geometric configuration is vital, and ANSYS ICEM CFD V.17 is used for meshing - grid element distribution. Performing a mesh grid-independent test to validate the accuracy of forecasting Nu and values yields an appropriate computation analysis outcome. Variable element sizes [four distinct values situated between 0.4 mm to 0.1 mm] were utilized to ascertain the ideal element cell size for the current operation. Table 2 outlines the validation outcomes. Figure 2 depicts the mesh

Table 1. Details of SAH using synthetic roughness units in a controlled environment

Geometrical parameters	Value and units
Length of the duct's entrance (L_1)	600 mm
Testing duct length (L_2)	1200 mm
Exit channel length (L_3)	300 mm
Size of the duct (W)	300 mm
The length of the conduit (H)	30 mm
Duct hydraulic diameter (D_h)	54 mm
Rib height (e)	10.2 mm
Pitch (P)	5,10, 15 and 20 cm
Aspect ratio (W/H)	10
Reynolds number	3000 – 15000 (8 values)

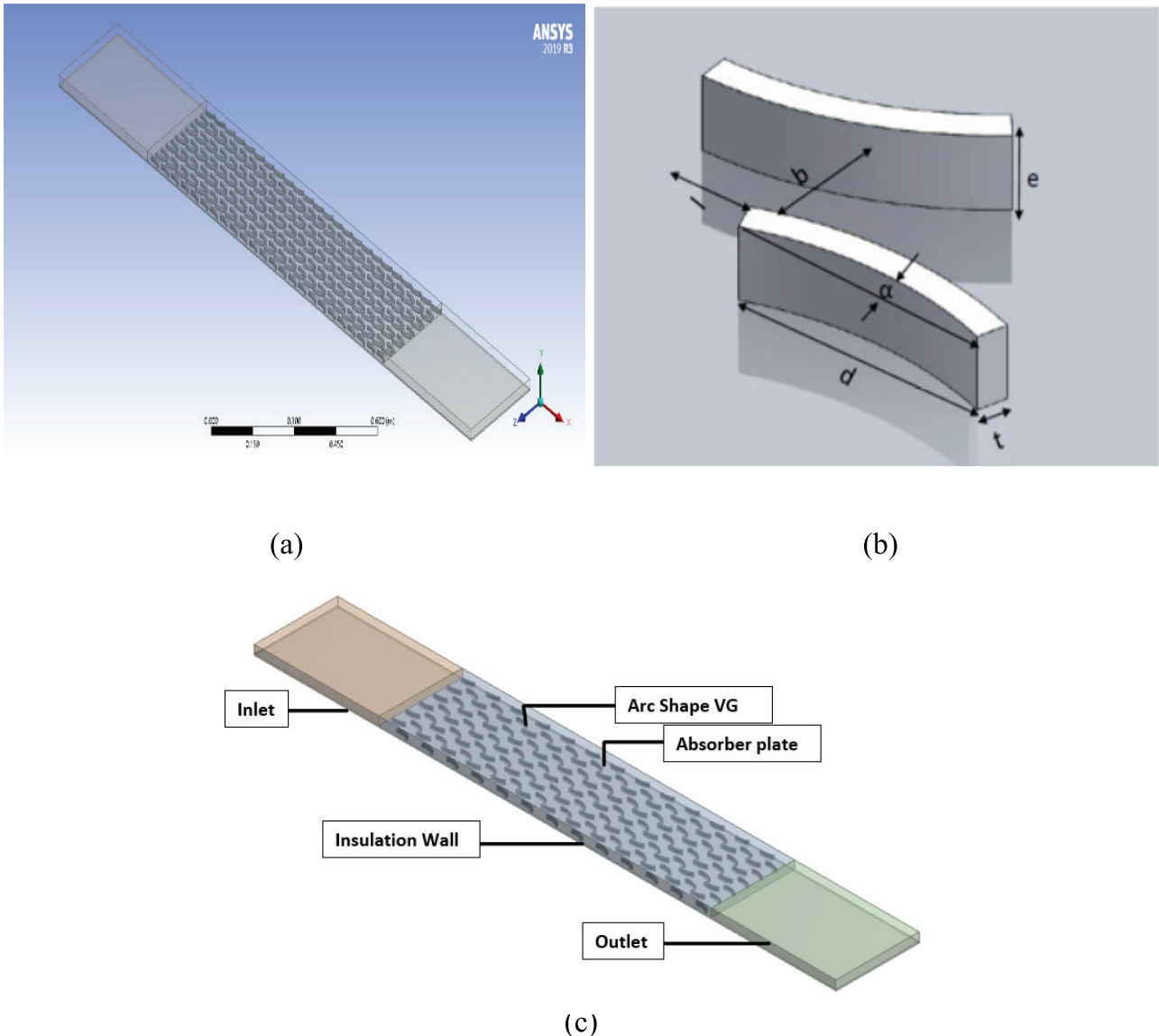


Figure1. (a) The geometry in ANSYS design modeler (b) Schematic view of VGs arc staggered (c) Computational domain.

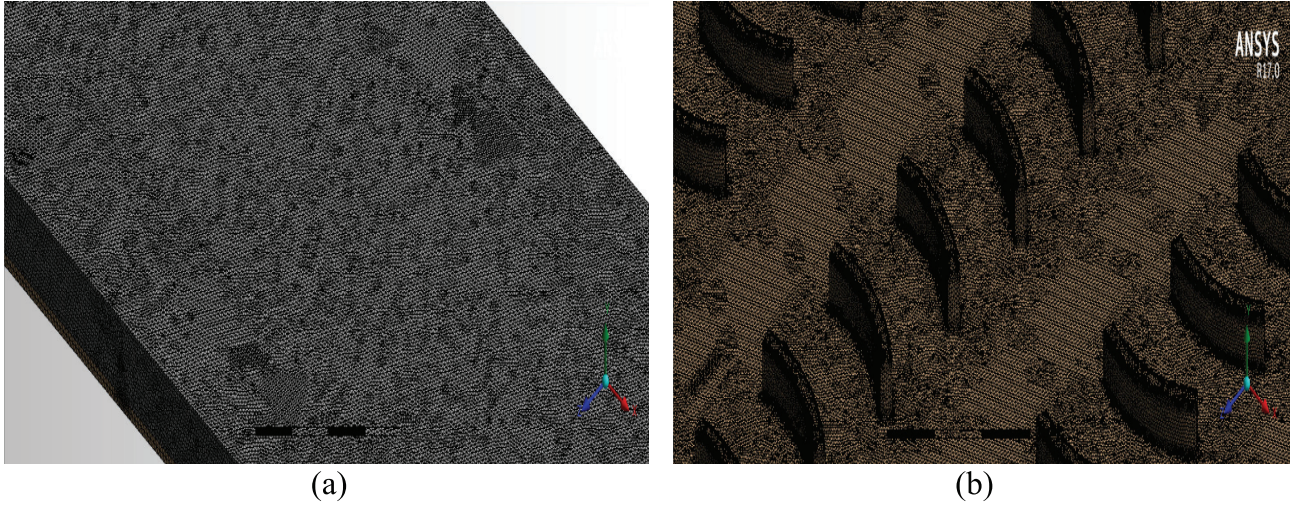


Figure 2. (a) Elements size of rough surface with arc shaped (b) The process of creating a computational mesh for different geometric shapes at $p = 10$ cm and $\alpha=60^\circ$.

Table 2. Grid-independent review

S. No	Size of the elements (mm)	Mesh element size	Nusselt number	% difference	Friction factor	% defference
1	0.4	4864379	132	5.2	2.55	3.2
2	0.3	6981321	158	4.1	2.51	2.1
3	0.2	8156465	177	3.5	2.48	1.9
4	0.1	9859884	200	2.1	2.3	1.2

formed for the VG arc shape with a discrete pitching of $p = 10$ cm and an attack angle of 60 degrees. According to the proposed element size, a nonuniform triangular grid is generated using a as well as convergent and fine mesh configurations engagement between 4864379 and 9859884 element cells. The largest Nu divergence was found in the 9859884-element cell, whereas the average Nu variation showed the least deviation at +2.1%. Consequently, the 9859884 element cell is utilized for analytical research.

Equation of Governance

Method of CFD involve utilizing numerical methods to resolve equations that ensure the conservation of mass, momentum, and energy. These solutions are obtained using the realizable (RNG) and k-ε models that are most effective when addressing eddy flows. To accurately describe the heat transfer process close to a wall with a steady heat flow, an enhanced wall manipulation is employed. Solving these equations with algorithms and numerical approaches. Below is a concise overview of the governing equations in three dimensions:

1. Continuity Equation (Conservation of Mass) [26]:

$$\frac{\partial \bar{u}_i}{\partial x_i} = 0 \quad (1)$$

2. Equation of momentum:

$$\rho \bar{u}_j \frac{\partial \bar{u}_i}{\partial x_j} = -\frac{\partial \bar{p}}{\partial x_j} + \frac{\partial}{\partial x_j} \left[\mu \left(\frac{\partial \bar{u}_i}{\partial x_j} + \frac{\partial \bar{u}_j}{\partial x_i} \right) - \rho \bar{u}_i \bar{u}_j \right] \quad (2)$$

Where the Reynolds stress tensor $-\rho \bar{u}_i \bar{u}_j$ is, evaluate through the Boussinesq approximation as:

$$-\rho \bar{u}_i \bar{u}_j = 2\mu_t \bar{S}_{ij} - \frac{2}{3} \rho k \delta_{ij} \quad (3)$$

Where δ_{ij} is Kronecker delta

3. Equation of energy:

$$\frac{\partial}{\partial x_i} (\rho u_i T) = \frac{\partial}{\partial x_j} \left((\Gamma + \Gamma_t) \frac{\partial T}{\partial x_j} \right) \quad (4)$$

$$\Gamma = \frac{\mu}{Pr}, \quad \Gamma_t = \frac{\mu_t}{Pr_t} \quad (5)$$

4. For the RNG k-ε model, the transport equation [27]:

$$\frac{\partial(\rho k)}{\partial t} + \frac{\partial(\rho u k)}{\partial x} = -\frac{\partial}{\partial t} \left[(a_k \mu_{eff}) \frac{\partial k}{\partial x} \right] + G_k + G_b - \rho \varepsilon - Y_M + S_k \quad (6)$$

$$\frac{\partial(\rho k)}{\partial t} + \frac{\partial(\rho u \epsilon)}{\partial x} = -\frac{\partial}{\partial t} \left[(a_k \mu_{eff}) \frac{\partial \epsilon}{\partial x} \right] + G_{1\epsilon} \frac{\epsilon}{k} (G_k + G_{3\epsilon} G_b) + G_{2\epsilon} \rho \frac{\epsilon^2}{k} - R_\epsilon + S_k \quad (7)$$

In the equation, the term of turbulence kinetic energy generation is due to mean velocity gradient it defines as

$$G_k = -\rho \overline{u_i u_j} \frac{\partial u_j}{\partial x_i} \quad (8)$$

Where μ_{eff} The term “effective turbulent viscosity” refers to the calculated value of the turbulent viscosity.

$$\mu_{eff} = \mu + \mu_t \quad (9)$$

Where μ_t turbulent viscosity is combining k and ϵ as following:

$$\mu_t = \rho C_\mu \frac{k^2}{\epsilon} \quad (10)$$

In addition, buoyancy and G_b respectively. $G_{1\epsilon} = 0.09$, $G_{3\epsilon} = 1.92$, In addition, $G_{2\epsilon} = 1.44$ that constant respectively and $a_k = 1.39$ $a_\epsilon = 1.39$ [28].

Boundary Conditions

To achieve the current geometry, The boundary conditions were implemented. At the beginning of the entrance, the temperature was 300 K and the velocity was constant. The Reynolds number is computed using Equation (12). The heat flow on the surface of the duct is equal to (1000 W/m²). As shown in Table 3. In addition, the air pressure at the exit remains constant at 1.013*10⁵ Pa, the standard atmospheric pressure as show in Table 4 properties of physical thermos hydraulic. The following is how the border condition is applied:

- i. At entry point in the X-direction

$$u = u_o, v = 0, T = T_o$$

- ii. At the Exit point

$$\frac{\partial u}{\partial x} = 0, \frac{\partial v}{\partial x} = 0, \frac{\partial T}{\partial x} = 0$$

- iii. Side and bottom walls

Table 3. Boundary condition for our work

Region	Limitation circumstances
Entry point	Velocity inlet
Exit point	Outflow
Upper wall of the duct	Wall
Lower surface of the duct	Wall

$$\dot{q} = 0$$

- iv. Upper wall (absorber plate)

$$u = 0, v = 0, q = 1000 \text{ W/m}^2$$

Data Reduction

A computational fluid dynamics (CFD) analysis of the Nu, f , and TPF rates is carried out in the publication. The following equation can be used to figure out the ave. Nu for the roughness of the artificial surface in solar air heaters:

$$Nu = \frac{h D_h}{k} \quad (11)$$

Reynolds number obtain from next equation [29]:

$$Re = \frac{\rho v D_h}{\mu} \quad (12)$$

The average f of a synthetic roughness SAH is found by [29]:

$$f = \frac{2}{L/D_h} \frac{\Delta P}{\rho v^2} \quad (13)$$

Where ΔP is the difference in pressure between the test portion and the rest of the heater.

An instrument for gauging the enhancement of heat transmission in a SAH with artificial roughness relative to a smooth channel is the thermal performance factor [29]:

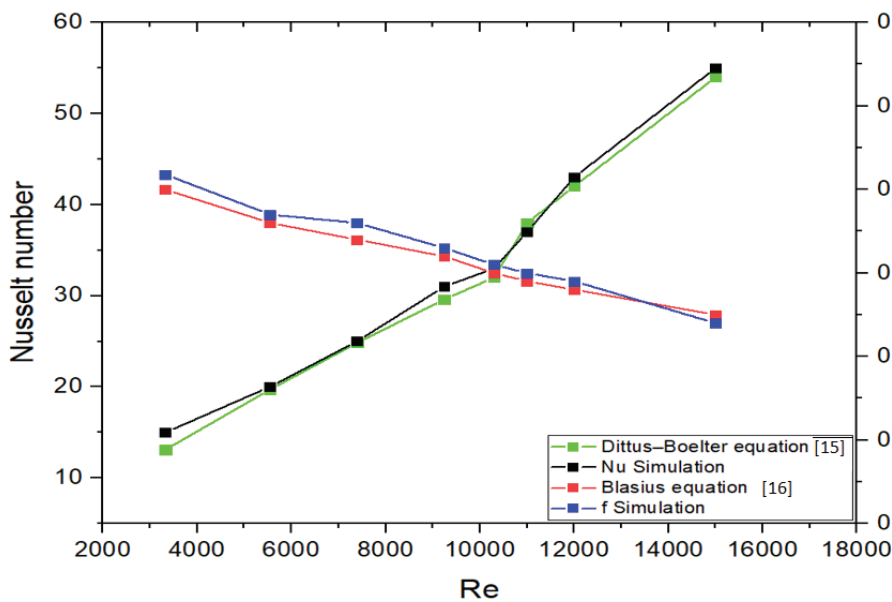
$$TPF = \frac{(Nu_r / Nu_s)}{(f_r / f_s)^{1/3}} \quad (14)$$

Table 4. The experimental setup and numerical simulation make use of the thermo-physical features of the material

Properties	Air	Aluminum	GI	Glass
Density (ρ)	1.225 kg/m ³	2719 kg/m ³	7870 kg/m ³	2600 kg/m ³
Specific heat (C_p)	1006.4 J/kg k	871 J/kg k	896 J/kg k	840 J/kg k
Viscosity(μ)	1.789e-05 kg/m-s	-----	-----	-----
Thermal conductivity (K)	0.0242 W/m ² -k	202.4 W/m ² -k	204.2 W/m ² -k	1.05 W/m ² -k

Table 5. Range of determined uncertainty error %

Parameter description	Symbol	Units	Uncertainty error %
Mass flow rate	\dot{m}	Kg/sec	(±0.0004155) 1.478%
Heat transfer coefficient	h	W/m ² K	(±0.50249) 5.02%
Reynolds number	Re	dimensionless	(±0.50249) 5.02%
Friction factor	f	dimensionless	(±0.0204) 2.04%
Nusselt number	N	dimensionless	(±0.0381) 3.81%

**Figure 3.** Validation of numerical results for flat plate SAH.

Uncertainty study

The error variance analysis was used to calculate the error percentage in the measurement equipment. If (Z) the beneficial property is dependent on the variables, it may be stated as follows. Table 5 contains the methods used to calculate experimental uncertainty in the measurement of Nu, Re, f, h, and \dot{m} .

$$\delta Z = \sqrt{\left(\frac{\partial Z}{\partial x_1} \delta x_1\right)^2 + \left(\frac{\partial Z}{\partial x_2} \delta x_2\right)^2 + \dots + \left(\frac{\partial Z}{\partial x_n} \delta x_n\right)^2}$$

Numerical Validation

This was done by comparing the corresponding rates found by correlation equations in rectangular channel smooth plates with the numerical results of the RNG, perturbation model for smooth stream quantities. Figure 3 shows the Nu and f as a function of Re, based on a comparison with the corresponding rates and numerical data for the uniform duct. The study's convergence was satisfactory

and suitable, according to the comparison. After receiving the associated Nusselt equation, the friction factor equation for a smooth channel can be obtained through the article's relationship.

Dittus-Boelter equation given by [30]:

$$Nu = 0.023Re^{0.8}Pr^{0.4} \quad (15)$$

Blasius equation given by [30]:

$$f = 0.316Re^{-0.25}, \text{ for } 3000 \leq R \leq 20000 \quad (16)$$

FINDINGS AND ANALYSIS

Heat Transfer

The impact of roughness pitch, angle of attack, Nusselt number, friction factor, and thermal enhancement factor on absorbent plates are investigated in this study using a staggered arc arrangement. The enhancement of heat transmission with the Nu and Nu ratio in Figure 4 and 5 illustrates the heat transfer through forced convection in a SAH, as indicated by the Nu. The figure shows a discrepancy

between the Nu and the Re. It is observed that when fixing $e/H=0.271$. As Re rises, so does the value of Nu. at the roughness parameters $p/H=1.667-6.667$ with an angle of attack of $30^\circ, 45^\circ$, and 60° . In addition, this is due to the increase in the Re That is, the turbulence increases and leads to the

formation of the ribs, breaking the thickness of the adjacent shear layer and in the direction of flow, a decrease in thermal resistance results in an increase in the amount of heat transfer, shown by the Nu. It should be noted that as p/H grows, Nu decreases because the regions in the higher p/H

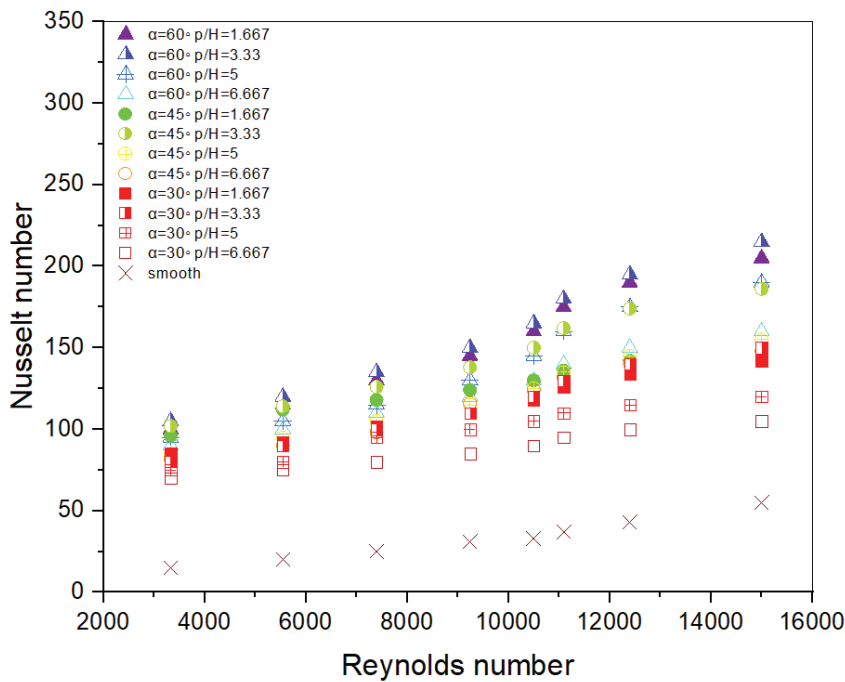


Figure 4. The Nu fluctuation in response to changes in Re, p/H , and angle of attack values.

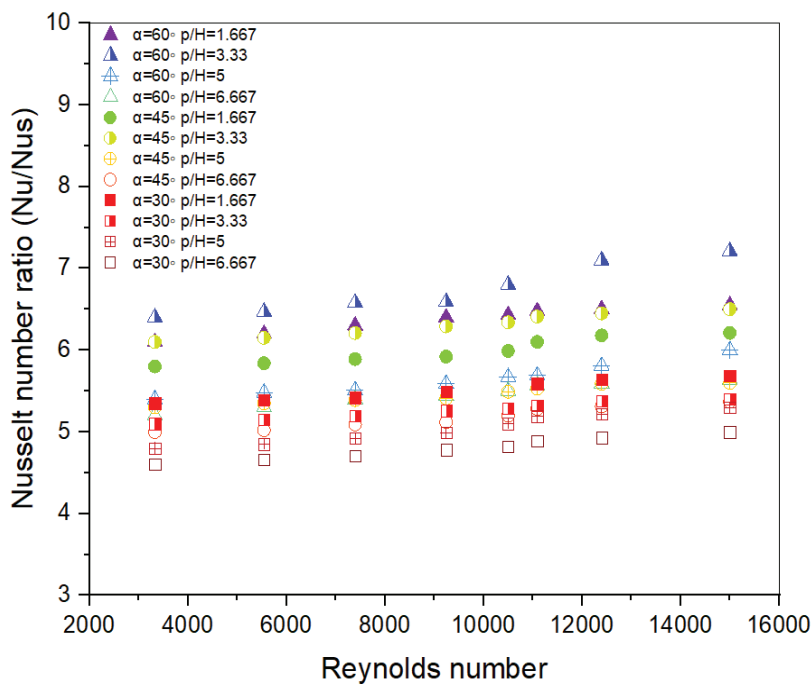


Figure 5. Nusselt number ratio variation with various Re.

values are few because the number of edges is small. It is noticed that when the values of the angle of attack increase, the flow becomes separated when a roughness element is present, leading to less heat transmission and the Nu worth increasing. Nu the highest possible value was 215 and Nu ratio maximum value was 7.21 at a p/H of 3.33, an angle of 60° , and a Re of 15000.

An increase in Re leads to an elevation in the kinetic energy of the turbulent flow, which in turn causes a greater rate of turbulent dissipation. This, in turn, causes the turbulence to become more intense and causes Nu to grow. Through Figure 6, it is possible to observe the kinetic energy contour diagrams in order to acquire a deeper comprehension of the activity of heat transfer. TKE is plotted for $p/H=3.33$ and angles of attack of 30° , 45° , and 60° with different rates of Re . Maximum TKE values are obtained

near the top of the staggered arc for a 60° angle of attack, where TKE decreases with increasing distance from the wall. An increase in TKE was observed up to a maximum value of (1.071, 5.112, and 7.481) m^2/s^2 for $Re = 3500$, 9000, and 15000, respectively. A high TDR region is observed at the beginning and end of the staggered arc. The obstruction of fluid flow leads to the release of TDR caused by eddy generators. However, the higher TDR value in the current is higher because of the second flow, which is caused by the generation of eddies. When TKE increases with Re , Nu increases.

Figure 7 presents the contour of the velocity vector in understanding the flow behavior along the YZ axis. To show the number of eddies generated at the angle of attack of 60° , and the step $p/H = 3.33$ and fixed $e/H = 0.271$ at $x/L=0.60$ begin of ribs and at $x/L=0.64$ end of ribs shows the best

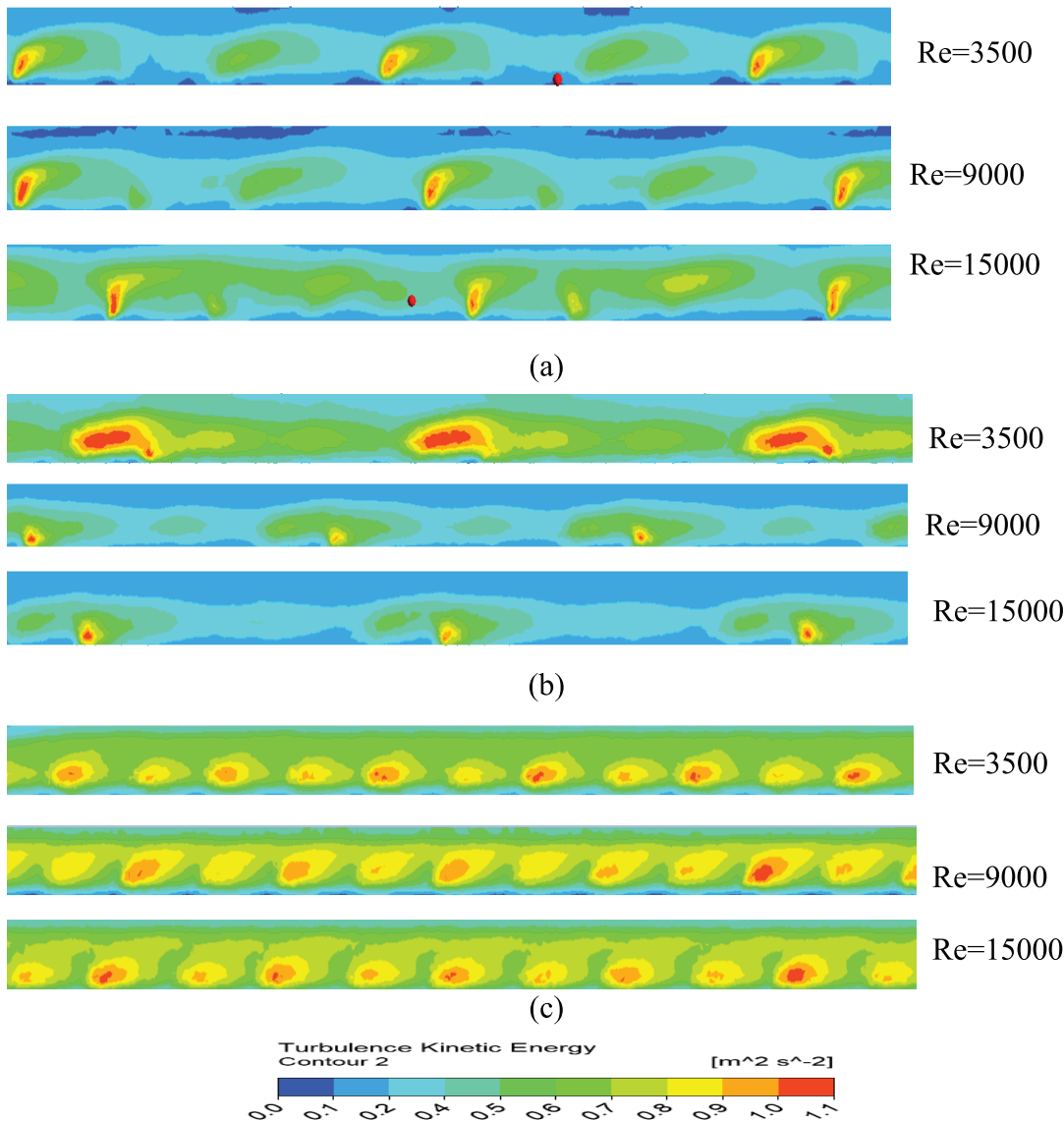


Figure 6. TKE contour for SAH at (a) angle of attack 30° (b) angle of attack 45° (c) angle of attack 60° .

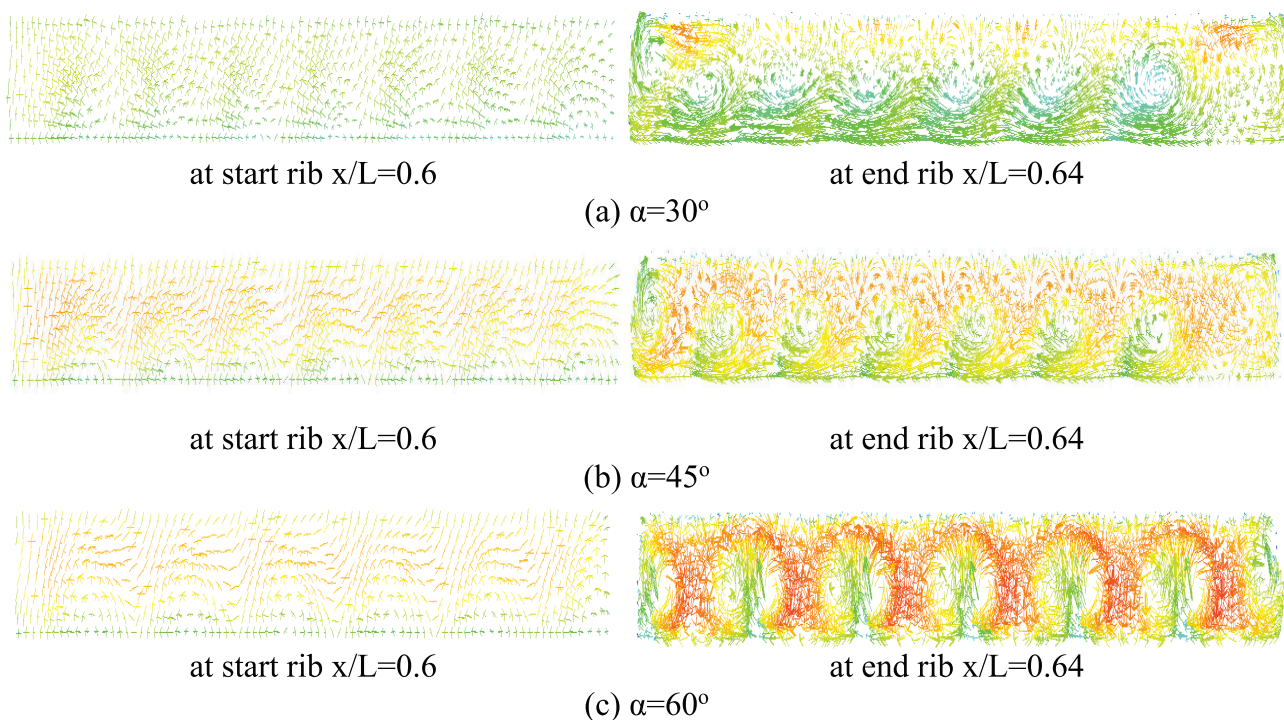


Figure 7. Velocity vector at YZ direction at Re=15000.

evaluation of the number of eddies generated that results in an augmentation of heat transfer. The rest of the figures (b & c) show the formation of vortices and their comparison with the angle of attack of 60° at Re=15000.

Figure 8 shows study investigates the influence of the assault angle on an arc-shaped staggered configuration of the absorber plate in a (SAH). The study demonstrates that the rib forms at specific relative pitch intervals and heights result in increased circulation in the flow direction. A robust vortex is formed in close proximity to the first rib Due to the acute angle at the apex and the additional inclination. The flow direction causes intense turbulence in close proximity to the wall surface, outcomes in an increased rate of heat transfer. The arc form with a 60-degree angle exhibits more pronounced representations compared to other arc shapes, suggesting the fact that a Nu rises as the Re increases, owing to enhanced fluid recirculation in the flow direction.

The impact that the angle of attack and the p/H ratio have on the SAH absorbent plate along the YZ axis is understood. And also, when Re = 15000, with an angle of attack of 60, a strong vortex was formed in the wall of the first rib because it was affected by the angle of attack at followed by a secondary vortex, which is located at the tip of the rib. As a result, this resulted in severe disturbances near the surface of the wall and thus a high rate of heat transfer. Figures 9 displaying the temperature distributions under the conditions mentioned p/H = 3.33, e/H=0.271, different case of angle of attack, and Re = 15000 with staggered arrangement. According to Figure 9, the temperature

distributions in the arc-shaped improved duct at an angle of 60° of contact are more evenly spread out compared to the other two examples. A greater disparity in temperature in the increased duct adjacent to the absorber plate promotes efficient thermal exchange between the absorber layer and the working fluid. Furthermore, the temperature distribution in the vicinity of the VGs alternates between warm and cold fluids, which promotes efficient heat transfer between the fluids. The current SAH improves heat transmission efficiency by rerouting cool fluid in the core flow, which cleans the heated absorber wall and lowers its temperature.

Friction Factor

The use of the VG staggered arc increases the amount of turbulence that is produced, disrupting the layer of viscous fluid near the surface. This disruption leads to a reduction in the frictional resistance, as the Re increases. The friction factor values of the rough layer are greater than those of the Unruffled layer, and the turbulence intensity becomes more with the Re, Figures 10 and 11 display the coefficient of friction values and the ratio of friction factor with the change of Re, with different parameters from p/H=1.667-6.667 and the angle of attack 30°, 45°, and 60°. Where it reached its highest value at p/H=3.33. The values of f and f/fs start decreasing due to the process of separating the flow that occurs under the rib and the process of reconnecting the shear layer at a lower p/H. When the values of the angle of attack increase, A rise in an angle of attack As a result of a growth in the coefficient of friction all the way up to its peak value at the angle of attack 60° and Commences retreat

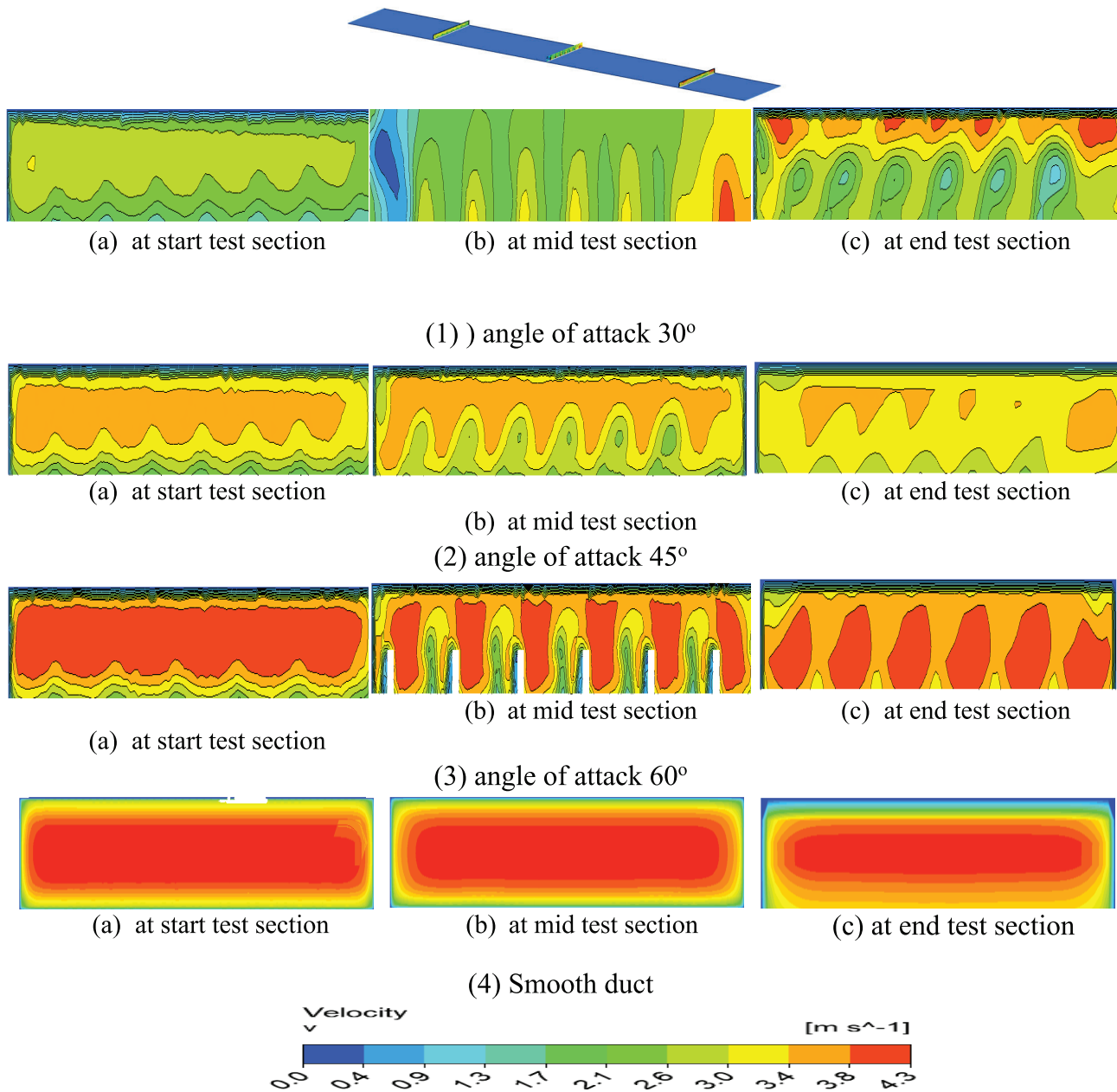


Figure 8. Contour of velocity profile at $Re=15000$ for (1) angle of attack 30° (2) angle of attack 45° (3) angle of attack 60° (4) Smooth duct.

The rib experiences the smallest angle of attack because of its large arc angle value, and a portion of it remains unaffected by the impediment. Where the highest value of $f = 2.5$ and $f/f_s = 3.39$ was obtained at $p/H = 3.33$ additional $e/H = 0.271$ at an angle of attack of 60°.

Thermal Performance Factor

The thermal performance factor is a measure that predicts the best improvement value in SAH in the coefficient of friction factor and heat transmission. It determines the optimum dimensions of the roughness used in the test and the arrangement that gives the optimum improvement in

heat transfer while reducing friction losses, in addition to the highest efficiency of SAH. The TPF method helps assess the relative Productivity of a the SAH compared to a main solar heater with a flat, absorbent surface. Where it was determined by an equation by Lewis [31]. In this numerical study, CFD provides the contrast between TPF and Re for SAH, supported by staggered arc ribs in Figure 12. With parameters at angles of 60, 45, and 30 degrees, the thermal performance work performance increases by 3.86, 3.73, and 2.7 percent, respectively, at $Re 15,000$.

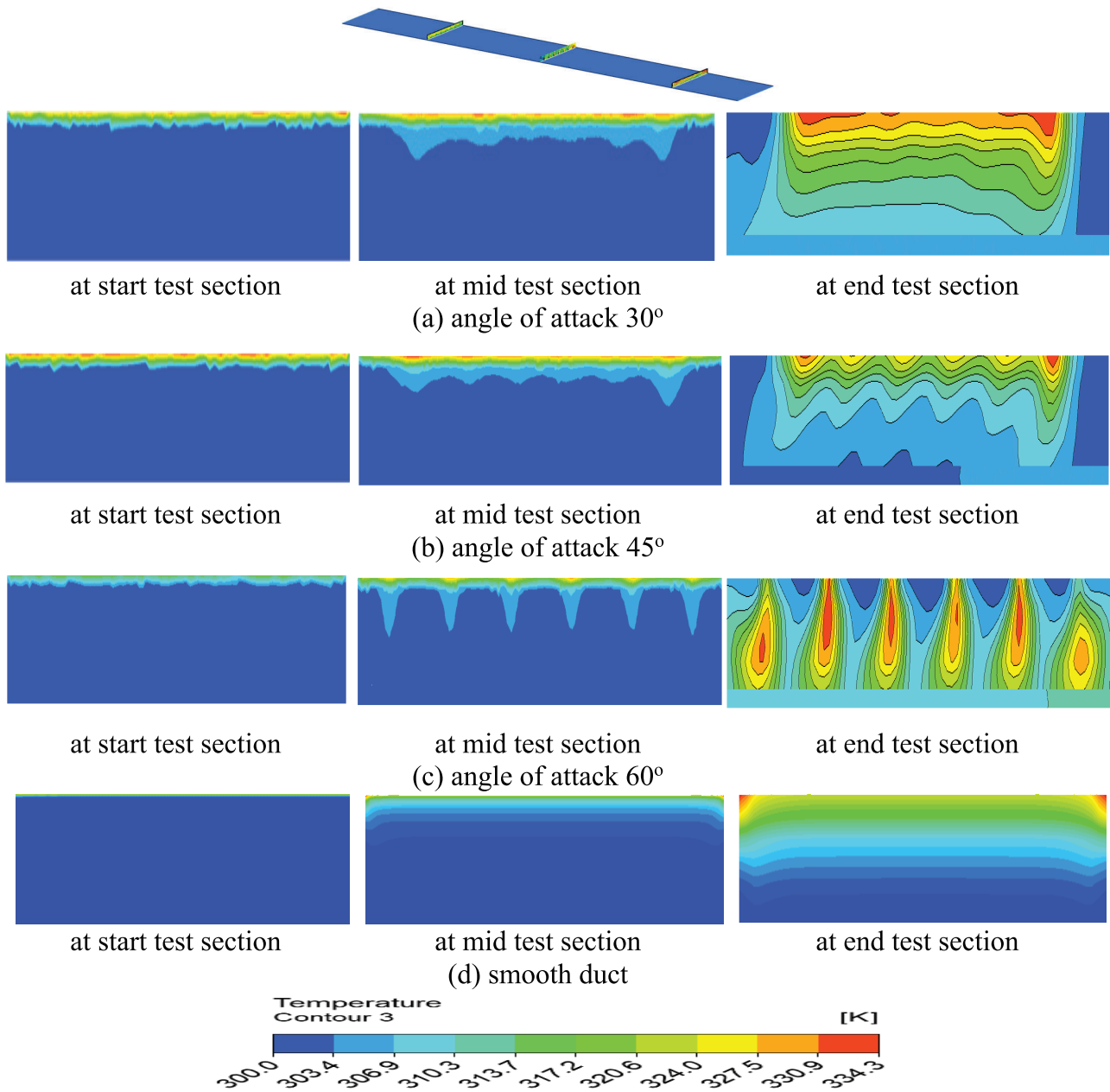


Figure 9. Temperature contour for Re15000 at (a) angle of attack 30° (b) angle of attack 45° (c) angle of attack 60° (d) Smooth duct.

Thermal performance of the arc-shaped VG staggered arrangement the current study involves a comparison with other studies. Multiple Arcs with Gap-Shaped (Pandey et al. [32]) and Multiple arc shaped (Singh et al. [33]). Table 6 presents a comparison of the highest TPF values obtained in the current investigation and those reported in previously published papers. The TPF of the current work was assessed in the table using the TPF formula, which is also employed to estimate TPF values for other devices mentioned previously. The current study exhibits a notably elevated TPF in comparison to equal Reynolds numbers (i.e.,

Re = 15000) and varied amounts for the angle of attack. An analysis to compare and contrast the current findings with the research conducted by Singh et al. [34], Pandey et al. [32], and Kumar et al. [35]. Figure 13 shows the study's highest TPF value is 3.86, with a minimum value of 2.7 at lower Reynolds numbers (Re). Nevertheless, as the value of Re climbs from 3000 to 15000, the TPF experiences a significant increase to 3.86, surpassing the previously declared maximum value by Singh et al. [34] and Pandey et al. [32] and Kumar et al. [35] i.e. 3.0, 3.4, and 3.8 respectively.

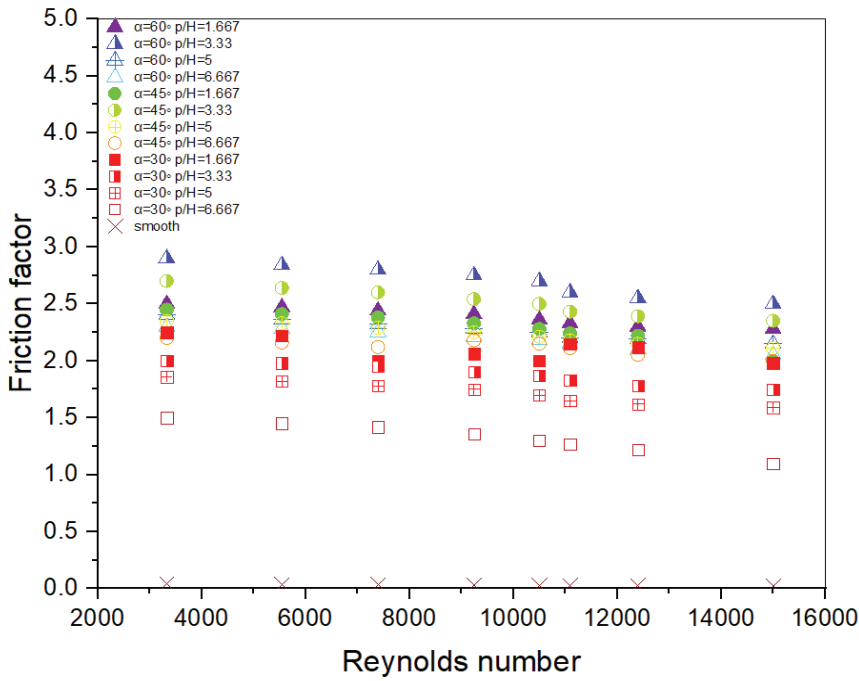


Figure 10. Changes in f as a function of Re at different p/H and attack angles.

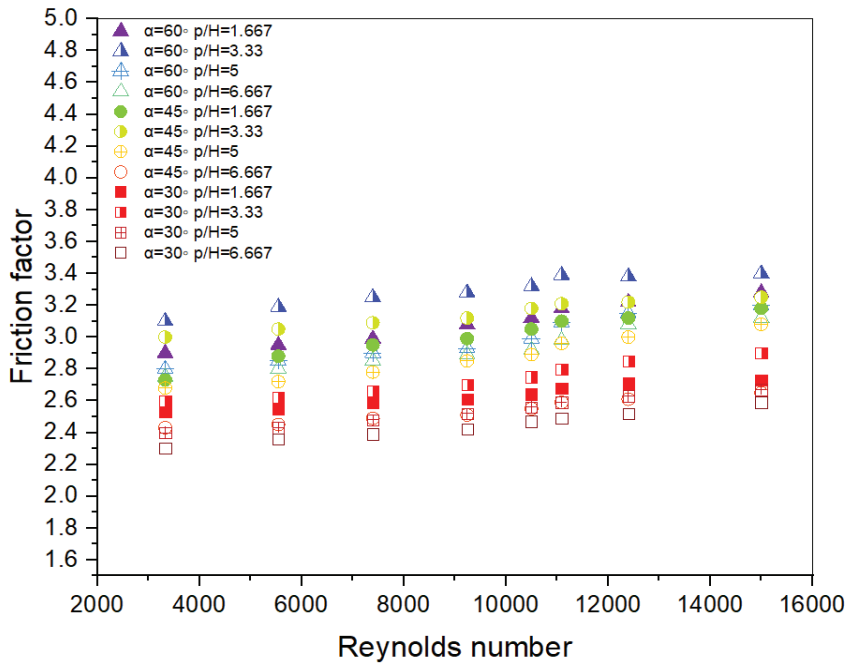


Figure 11. Variation of f ratio with Re at differed p/H and angle of attack.

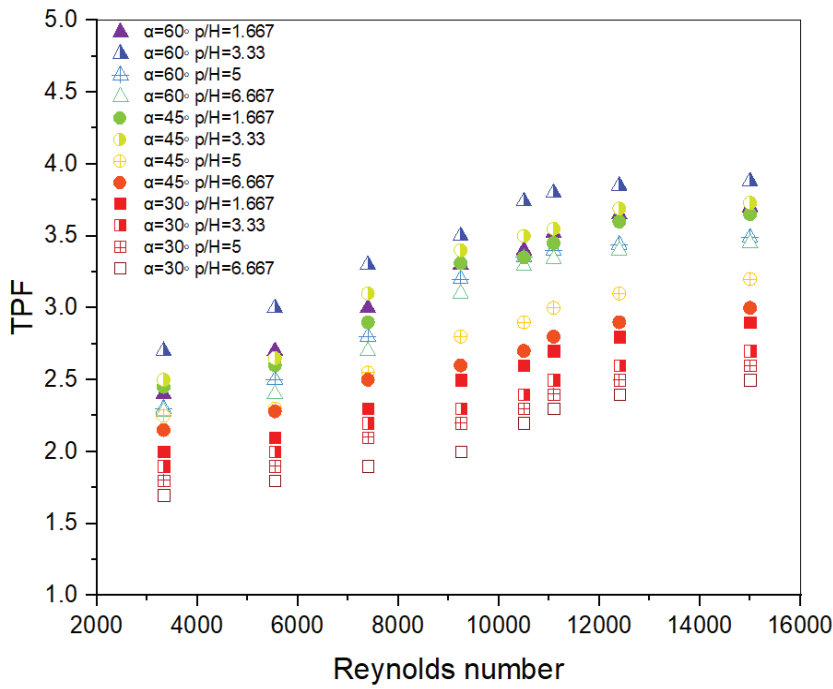


Figure 12. Changes in TPF as a function of Re at various p/H and attack angles.

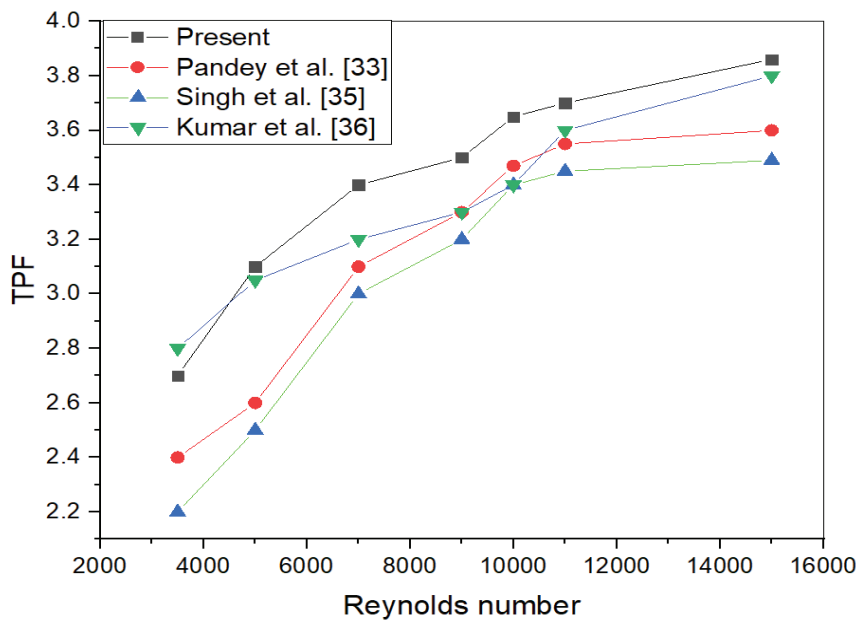


Figure 13. The TPP values of this research are compared to those of earlier studies.

Table 6. Evaluation of the computational fluid dynamics (CFD) analysis in relation to prior research

Reference	Geometry	Maximum TPF
Pandey et al. [32]	Multiple Arcs with Gap-Shaped	3.6
Singh et al. [33]	Multiple arc shaped	3.4
Present study	Arc shape staggered VGs	3.88

CONCLUSION

The ANSYS Fluent program was used to predict the efficiency of a SAH with arc-shaped ribs using a three-dimensional numerical model. The results were evaluated using streamlines, the average Nusselt number, the average friction coefficient, and the thermal-hydraulic performance parameter. A CFD investigation was conducted using the RNG $k-\epsilon$ turbulence model with different Reynolds numbers, p/H , angle of attack, and α . The study found significant findings:

1. This study's CFD analytical results were confirmed by the correct experimental outcomes anticipated by the RNG- k , which was validated for a smooth duct.
2. Nusselt number increase with Re . At $p/H = 3.33$ and an angle of 60° at $Re = 15000$, and $e/H=0.271$ the most important factors of Nu and Nu ratio were 215 and 7.21 time that of smooth duct for same p/H and e/H , respectively.
3. The f reduces as the Re augment. Where the highest value of $f = 2.5$ and $f/fs = 3.39$ was obtained at $p/H = 3.33$ and $e/H = 0.271$ at an angle of attack of 60° .
4. It found arc staggered VGs at $p/H = 3.33$ and an angle of 60° at $Re = 15000$ provide maximum thermal performance factor 3.88 for augmentation heat transfer.

NOMENCLATURE

D_h	Hydraulic diameter (m)
I	Solar radiation intensity (W/m^2)
T	Temperature (k)
k	Heat transfer coefficient ($W/m^2 k$)
α	Angle of attack ($^\circ$)
TPF	Thermal performance factor
SAH	Solar air heater
VGs	Vortex generator
TKE	Turbulent kinetic energy
GI	Galvanized iron

Dimensionless

Re	Reynolds number
Nu_s	Nusselt number(smooth)
Nu	Average Nusselt number
f_s	Friction factor (smooth)
f	Average Friction factor
P	Pitch (mm)
e	Height of rectangular (mm)
p/H	respective rough of pitch
l/H	respective rough of length
d/H	Length of the respective rough
e/H	Height of the respective rough
b/H	the distance between each arc

Greek Symbols

ρ	Density (Kg/m^3)
μ	Dynamic viscosity ($N.s/m^2$)
\dot{m}	mass flow rate

AUTHORSHIP CONTRIBUTIONS

Authors equally contributed to this work.

DATA AVAILABILITY STATEMENT

The authors confirm that the data that supports the findings of this study are available within the article. Raw data that support the finding of this study are available from the corresponding author, upon reasonable request.

CONFLICT OF INTEREST

The author declared no potential conflicts of interest with respect to the research, authorship, and/or publication of this article.

ETHICS

There are no ethical issues with the publication of this manuscript.

REFERENCES

- [1] Hasan KS, Khwayyir HHS, Abd Al-Wahid WA. Experimental investigation of the flame stability map (operating window) by using a tangential swirl burner for the confinement and unconfinement space. IOP Conf Ser Mater Sci Eng 2020;928:022016. [\[CrossRef\]](#)
- [2] Hasan KS. Study operation of steam generation system using different fuels [dissertation]. Al-Furat Al-Awsat Technical University; 2020.
- [3] Kannan N, Vakeesan D. Solar energy for future world: A review. Renew Sustain Energy Rev 2016;62:1092-1105. [\[CrossRef\]](#)
- [4] Yousif AH, Khudhair MR. Enhancement heat transfer in a tube fitted with passive technique as twisted tape insert-A comprehensive review. Am J Mech Eng 2019;7:20-34.
- [5] Yousif A. Numerical analysis for flow and heat transfer in new shapes of corrugated channels. J Babylon Univ Sci. 2015;23:126191925.
- [6] Yousif AH. An effect of orientation on heat transfer characteristic from triangular cylinder by using winglets. Int J Mech Prod Eng Res Dev 2018;9:119-130. [\[CrossRef\]](#)
- [7] Sachdev T, Vivek G, Tiwari A. Comparative thermal analysis of applications using novel solar air heater with u-shaped longitudinal fins: suitable for coastal regions. J Therm Eng 2021;7:1174-1183. [\[CrossRef\]](#)
- [8] Yıldırım C. Theoretical investigation of a solar air heater roughened by ribs and grooves. J Therm Eng 2018;4:1702-1712. [\[CrossRef\]](#)
- [9] Garg HP. Solar energy: Fundamentals and applications. Tata McGraw-Hill Education; 2000.

- [10] Jovini M, Khoshvaght-Aliabadi M, Sardarabadi M. Experimental study of utilizing springs on absorber plate of solar air heaters: Subjected to axial-flow and cross-flow. *Sustain Energy Technol Assess* 2022;53:102661. [\[CrossRef\]](#)
- [11] Ifrim VC, Pop T. Review of thermal performance enhancement of solar air heater using shapes on absorber plate. 2022 International Conference on Development and Application Systems (DAS) 2022:19-27. [\[CrossRef\]](#)
- [12] Alam T, Meena CS, Balam NB, Kumar A, Cozzolino R. Thermo-hydraulic performance characteristics and optimization of protrusion rib roughness in solar air heater. *Energies* 2021;14:3159. [\[CrossRef\]](#)
- [13] Kumar A, Saini RP, Saini JS. Heat and fluid flow characteristics of roughened solar air heater ducts-A review. *Renew Energy* 2012;47:77-94. [\[CrossRef\]](#)
- [14] Hans VS, Saini RP, Saini JS. Performance of artificially roughened solar air heaters-A review. *Renew Sustain Energy Rev* 2009;13:1854-1869. [\[CrossRef\]](#)
- [15] Bhushan B, Singh R. A review on methodology of artificial roughness used in duct of solar air heaters. *Energy* 2010;35:202-212. [\[CrossRef\]](#)
- [16] Chand NV, Kumar V, Sehgal AK. An analysis of a duct with different vortex generators for performance enhancement of a solar air heater: Computational fluid dynamics (CFD) BT. *Adv Fluid Ther Eng* 2019:637-645. [\[CrossRef\]](#)
- [17] Yadav AS, Sharma A. Experimental investigation on heat transfer enhancement of artificially roughened solar air heater. *Heat Transf Eng* 2022:1-14. [\[CrossRef\]](#)
- [18] Jin D, Quan S, Zuo J, Xu S. Numerical investigation of heat transfer enhancement in a solar air heater roughened by multiple V-shaped ribs. *Renew Energy* 2019;134:78-88. [\[CrossRef\]](#)
- [19] Luo L, Wen F, Wang L, Sundén B, Wang S. On the solar receiver thermal enhancement by using the dimple combined with delta winglet vortex generator. *Appl Therm Eng* 2017;111:586-598. [\[CrossRef\]](#)
- [20] Tamna S, Skullong S, Thianpong C, Promvong P. Heat transfer behaviors in a solar air heater channel with multiple V-baffle vortex generators. *Sol Energy* 2014;110:720-735. [\[CrossRef\]](#)
- [21] Fadala GM, Yousef AH. The effect of artificial roughness on performance of solar air heater (SAH): A review study. *AIP Conf Proc* 2023;2776:50008. [\[CrossRef\]](#)
- [22] Zhang L, et al. Heat transfer enhancement by streamlined winglet pair vortex generators for helical channel with rectangular cross section. *Chem Eng Process Intensif* 2020;147:107788. [\[CrossRef\]](#)
- [23] Gupta A, Roy A, Gupta S, Gupta M. Numerical investigation towards implementation of punched winglet as vortex generator for performance improvement of a fin-and-tube heat exchanger. *Int J Heat Mass Transf* 2020;149:119171. [\[CrossRef\]](#)
- [24] Li M, Qu J, Zhang J, Wei J, Tao W. Air side heat transfer enhancement using radiantly arranged winglets in fin-and-tube heat exchanger. *Int J Therm Sci* 2020;156:106470. [\[CrossRef\]](#)
- [25] Promvong P, Skullong S. Thermo-hydraulic performance in heat exchanger tube with V-shaped winglet vortex generator. *Appl Therm Eng* 2020;164:114424. [\[CrossRef\]](#)
- [26] Bergman TL, Incropera FP, Dewitt DP, Lavine AS. *Fundamentals of Heat and Mass Transfer*. John Wiley & Sons; 2011.
- [27] Lam CK, Bremhorst K. A modified form of the $k-\epsilon$ model for predicting wall turbulence. *J Fluids Eng* 1981;103(3):456-460. [\[CrossRef\]](#)
- [28] Versteeg HK, Malalasekera W. *An Introduction to Computational Fluid Dynamics: The Finite Volume Method*. Pearson Education; 2007.
- [29] Varun, Saini RP, Singal SK. Investigation of thermal performance of solar air heater having roughness elements as a combination of inclined and transverse ribs on the absorber plate. *Renew Energy* 2008;33:1398-1405. [\[CrossRef\]](#)
- [30] Incropera FP, Dewitt DP, Bergman TL, Lavine AS. *Introduction to Heat Transfer*. John Wiley & Sons; 1996. pp. 280-284.
- [31] Lewis MJ. Optimising the thermohydraulic performance of rough surfaces. *Int J Heat Mass Transf* 1975;18:1243-1248. [\[CrossRef\]](#)
- [32] Pandey NK, Bajpai VK, Varun. Heat transfer and friction factor study of a solar air heater having multiple arcs with gap-shaped roughness element on absorber plate. *Arab J Sci Eng* 2016;41:4517-4530. [\[CrossRef\]](#)
- [33] Singh AP, Varun, Siddhartha. Heat transfer and friction factor correlations for multiple arc shape roughness elements on the absorber plate used in solar air heaters. *Exp Therm Fluid Sci* 2014;54:117-126. [\[CrossRef\]](#)
- [34] Singh S, Chander S, Saini JS. Heat transfer and friction factor correlations of solar air heater ducts artificially roughened with discrete V-down ribs. *Energy* 2011;36:5053-5064. [\[CrossRef\]](#)
- [35] Kumar R, Goel V, Singh P, Saxena A, Kashyap AS, Rai A. Performance evaluation and optimization of solar assisted air heater with discrete multiple arc shaped ribs. *J Energy Storage* 2019;26:100978. [\[CrossRef\]](#)